THE JOURNAL OF PHYSICAL CHEMISTRY C

Article

Cite This: J. Phys. Chem. C 2019, 123, 6090−6096

pubs.acs.org/JPCC

Characterizing the Incorporation of DNA into Single NIPAm Hydrogel Nanoparticles with Surface Plasmon Resonance Imaging Measurements

Brandon M. Matthews, Adam M. Maley,† Kellen M. Kartub, and Robert M. Corn*

Department of Chemistry, University of California-Irvine, Irvine, California 92697, United States

Supporting Information

ABSTRACT: *N*-Isopropylacrylamide-based hydrogel nanoparticles (HNPs) that incorporate 30 mer single-stranded DNA (ssDNA) oligonucleotides were synthesized and characterized with single-nanoparticle surface plasmon resonance imaging (SPRI) microscopy, dynamic light scattering, transmission electron microscopy, and fluorescence measurements. The synthesized HNPs had an averaged diameter of 230 nm and exhibited a large (5−10×) increase in the average single-nanoparticle SPRI refractive index (Δ% R_{NP}), as compared with HNPs without DNA. A combination of SPRI and fluorescence measurements was used to measure the uptake of approximately 20 000 complementary ssDNA into each HNP, resulting in a Langmuir isotherm adsorption coefficient of 4.89×10^8 M^{-1}. Single-nanoparticle SPRI measurements also showed that approximately 35% of the incorporated ssDNA was accessible for both hybridization uptake and enzymatic hydrolysis using exonuclease I. We attribute the presence of an inactive ssDNA population in the nanoparticle to a combination of acrylamide Michael addition reactions with adenine, cytosine, and guanine nucleotides, as well as the possible formation of self-complementary secondary structures in the polymerized ssDNA.

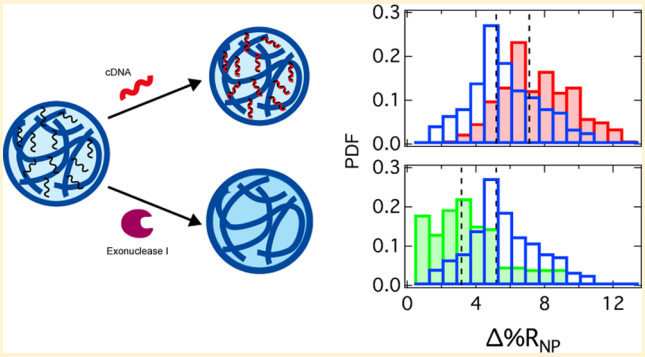

INTRODUCTION

A variety of polymeric hydrogel nanoparticles (HNPs) are currently employed as nanoscale materials for the uptake, transport, collection, and release of various therapeutics and biomarkers, including drug molecules, peptides, proteins, nucleic acids, antibodies, and even small metallic nanoparticles.[1−10] For example, *N*-isopropylacrylamide (NIPAm)-based hydrogel nanoparticles that incorporate various ratios of *tert*-butyl and acrylic acid (AAc) have been optimized for the specific uptake and delivery of the polypeptide melittin, the active component in honey bee venom,[11] and the toxins in elapid snake venom.[12] NIPAm-based HNPs have also been engineered to incorporate bioaffinity binding sites,[13] such as mannose sugars for the specific uptake of lectins.[14]

To further explore the loading capabilities of hydrogel nanoparticles, we synthesize 230 nm NIPAm-based nanoparticles that incorporate single-stranded DNA (ssDNA) directly into the polymer, forming DNA−HNPs, and then quantitate their ssDNA binding affinity and exonuclease activity through a combination of single-nanoparticle surface plasmon resonance imaging (SPRI) microscopy, fluorescence measurements, dynamic light scattering (DLS), and transmission electron microscopy (TEM). The incorporation of ssDNA is an obvious choice as a versatile binding site due to its ability to hybridize to complementary nucleic acid sequences with excellent specificity,[15] to be hydrolyzed[16] or ligated[17] with various high-efficiency DNA enzymes, and to fold into configurations that either bind molecular targets or exhibit enzymatic reactivity, releasing potential cargo.[18−20] NIPAm-based hydrogels that incorporate and release ssDNA using these mechanisms have been used extensively in a thin film format, primarily on planar surfaces, but also in a core−shell nanoparticle format.[4,21−23] For example, DNA−HNPs were used in the uptake, delivery, and release of small interfering RNA to infected cells.[9,24,25]

Figure 1 incorporates a mixture of acrylamide-modified species in ratios similar to those used in our previous work[14] but with the addition of acrylic phosphoramidite-modified 30 mer ssDNA. Acrylamide has demonstrated reactivity toward DNA, most notably via a Michael addition reaction with guanine, cytosine, and adenosine nucleotides.[26,27] These types of Michael addition reactions cause acrylamide to form DNA adducts, which have shown to affect the biological activity of regulatory systems.[28−30] In the case of DNA−HNP formations, this interaction could give rise to additional polymerization sites, aiding in the incorporation of DNA as a whole.[30] We theorize that this additional acrylamide cross-linking accounts for only observing approximately 35% of the incorporated

Received: January 15, 2019
Revised: February 22, 2019
Published: February 22, 2019

DOI: 10.1021/acs.jpcc.9b00444
J. Phys. Chem. C 2019, 123, 6090−6096

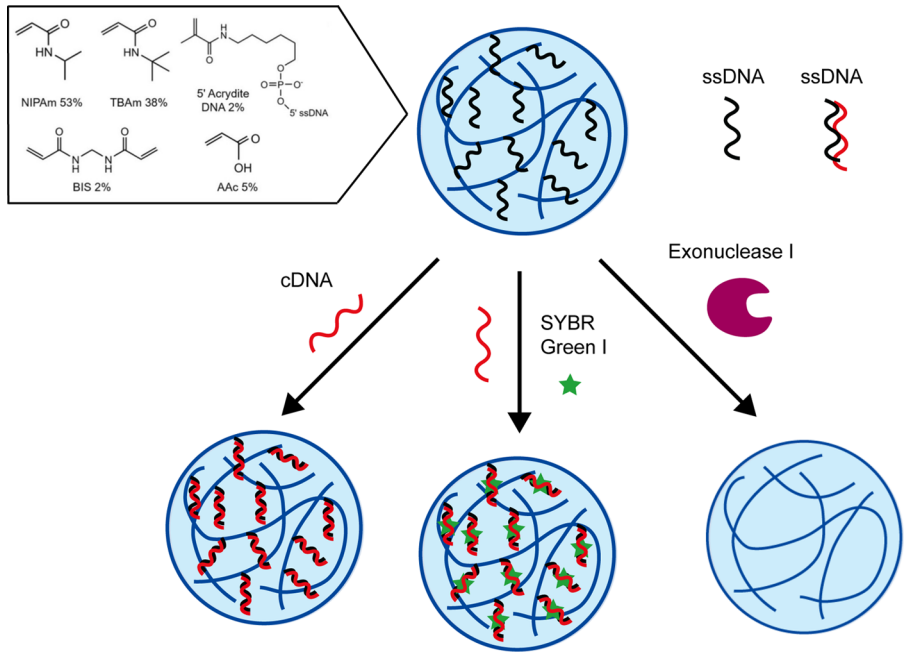

Figure 1. DNA-incorporated hydrogel nanoparticles (HNPs) were composed of *N*-isopropylacrylamide (NIPAm, 53 mol %), *N*-*tert*-butylacrylamide (TBAm, 38 mol %), acrylic acid (AAc, 5 mol %), *N*,*N*′-methylenebis(acrylamide) (BIS, 2 mol %), and 5′-modified acrylic phosphoramidite DNA (2 mol %). Following purification, incorporated DNA was tested to demonstrate accessibility and chemical activity, via specific complementary sequence hybridization to form double stranded DNA (dsDNA), fluorescent dyeing, and enzymatic activity through DNA hydrolysis.

ssDNA being available for hybridization with complementary ssDNA or enzymatic exonuclease activity.

METHODS

Hydrogel Nanoparticle Materials. *N*-Isopropylacrylamide (NIPAm), acrylic acid (AAc), sodium dodecyl sulfate (SDS), and ammonium persulfate (APS) were obtained from Sigma-Aldrich, Inc. (St. Louis, MO). *N*,*N*-Methylenebis(acrylamide) (BIS) was obtained from Fluka (St. Louis, MO). *N*-*tert*-Butylacrylamide (TBAm) was obtained from Acros Organics (Geel, Belgium). All DNAs were purchased from Integrated DNA Technologies (Coralville, IA). NIPAm was recrystallized from hexane before use. All other chemicals were used as received.

Hydrogel Nanoparticle Synthesis. HNP synthesis was adapted from the procedure detailed in Cho et al.[11] The monomers NIPAm (53 mol %), TBAm (38 mol %), AAc (5 mol %), and BIS (2 mol %) were dissolved in 1.7 mL of nanopure water in a round-bottom flask for a total monomer concentration of 21 mM. TBAm was dissolved in 50 μL of ethanol before addition to the monomer solution. The surfactant SDS (0.25 mg) was also added to the monomer solution to control the nanoparticle size. Nitrogen gas was bubbled through the solution for 30 min. Following the addition of a 100 μL aqueous solution containing 1 mg of APS, the polymerization reaction was carried out in an oil bath preset to 60 °C. After 30 min of reaction time, 1.3 μmol (1 mM aqueous solution) of DNA was added to the reaction flask via syringe, and the polymerization reaction was allowed to proceed for an additional 2.5 h under a nitrogen atmosphere. The resulting solution was purified by dialysis using a 12−14 kDa molecular weight cutoff dialysis membrane against an excess amount of nanopure water (changed three times a day) for 3 days. Hydrogel nanoparticle size distribution and concentration were measured in aqueous solutions at 25 °C on a dynamic light scattering (DLS) instrument equipped with Zetasizer software (Zetasizer Nano ZS, Malvern Instruments Ltd., Worcestershire, U.K.) and a NanoSight NS300 nanoparticle tracking and analysis microscopy system (Malvern Panalytical). Cryo-TEM images were obtained using 3 μL of sample solution applied on a glow-discharged Quantifoil grid (Quantifoil, R2/2) and then loaded on a Leica EMGP plunger (Leica Biosystem). The grid was quickly plunged into liquid propane after blotting away the excess liquid, and the hydrogel particles were then embedded in a thin layer of vitrified ice on the grid. The cryo-grid was then transferred into a JEM-2100F electron microscope using a Gatan cryo-transfer holder (Gatan, Inc.). The electron microscope was operated at 200 kV with a field emission gun, and the specimen was examined under a minimum dose system. The images were recorded on a OneView camera (Gatan, Inc.) at 40 000× magnification, corresponding to 0.28 nm per pixel at specimen space.

Substrate Preparation. The Au substrates were coated by the thermal vapor deposition of a 1 nm Cr adhesion layer and 45 nm Au onto borosilicate No. 1.5 coverslips (Fisherbrand, Pittsburgh, PA). The Au surface was immobilized with 1-undecanethiol (C11) by immersing the Au substrate into a 1 mM C11/EtOH solution. The Au surface was partitioned using adhesive silicon isolation wells (Electron Microscopy Sciences, Hatfield, PA).

SPRI Microscopy Measurements. The SPRI microscope setup is described in a previous publication.[31] The microscope was built into the frame of an IX51 inverted microscope (Olympus, Tokyo, Japan). A 1 mW, 814 nm diode laser (Melles Griot, Carlsbad, CA) was expanded and collimated using a spatial filter (Newport Corp., Newport Beach, CA). The beam was polarized and focused with a lens (f = 200 mm) and then directed onto the back focal plane of a 100× 1.49

DOI: 10.1021/acs.jpcc.9b00444
J. Phys. Chem. C 2019, 123, 6090−6096

Table 1. ssDNA Sequences Incorporated into Various Batches of DNA−HNPs

label	DNA sequence
D1	5′-acrydite- TCT GTG ATT AGC GAT TGT TTA GGT GTA TGC-3′
D1c	5′-GCA TAC ACC TAA ACA ATC GCT AAT CAC AGA-3′
D1nc	5′-CGA AAT CCA GAC ACA TAA GCA CGA ACC GAA-3′
D2	5′-acrydite- TTT TTT TTT TTT TTT TTT TCT TCA TTG TTT-3′
D3	5′-acrydite-TTT TTT TTT TTT TTT TTT TTT TTT TTT TTT-3′
D4	5′-acrydite-AAA AAA AAA AAA AAA AAA AAA AAA AAA AAA-3′

high numerical aperture objective (Olympus). The beam was directed upward near the edge of the objective by a gold-coated knife-edge mirror (Thorlabs, Newton, NJ). The reflected image was passed out the other side of the objective and acquired by an Andor Neo sCMOS camera (South Windsor, CT). Each 3 s reflectivity image was acquired by accumulating 30, 11 bit, 0.1 s exposures.

Enzymatic SPRI Measurements. Exonuclease I (5 μL of 20 U/μL; New England Biolabs) was added to 1−10 diluted 10× reaction buffer (67 mM glycine−KOH, 6.7 mM $MgCl_2$, 10 mM β-ME, pH 9.5) and a 1−10 stock-diluted D1-HNP solution to a final volume of 500 μL in nanopure water. The solution was incubated at 37 °C for 1 h before carrying out three wash cycles similar to the fluorescence measurements described above. After the final wash, the solution was then resuspended to a final volume of 50 μL.

RESULTS AND DISCUSSION

Synthesis and Characterization of DNA−HNPs. Four types of DNA−HNPs were synthesized and then characterized via a combination of DLS, TEM imaging, fluorescence measurements, and single-nanoparticle surface plasmon resonance imaging (SPRI) microscopy. DNA−HNP size distribution was obtained by DLS and confirmed using TEM imaging. Through the combination of fluorescence loss measurements and nanoparticle tracking measurements, an incorporated DNA concentration of approximately 22 000 ± 1000 fluorophores per nanoparticle was found.

The primary DNA sequence used for DNA−HNPs analysis is denoted D1; its complementary sequence is labeled D1c and control sequence D1nc. To analyze potential influences of the nucleotides used during the synthesis, three additional sequences were also used: a modified 30 mer sequence from Lilienthal et al.,[18] a poly-T sequence, and a poly-A sequence, denoted D2, D3, and D4, respectively. All sequences used are summarized in Table 1. A large amount of D1 ssDNA was found incorporated into the HNPs, suggesting some degree of cooperativity between the ssDNA and the acrylamide polymerization process. SPRI nanoparticle measurements showed that the resultant DNA−HNPs were able to specifically hybridize complementary 30 mer ssDNA (D1c) with nanomolar binding efficiency and were easily hydrolyzed by the DNA enzyme exonuclease I.

The primary method used to characterize the activity of the DNA−HNPs was near-infrared single-nanoparticle SPRI microscopy. This relatively new microscopic single-nanoparticle method has been employed recently to detect and characterize distributions of polymeric, oxide, and metal nanoparticles based on the nanoparticle's integrated refractive index.[32−35] In a single-nanoparticle SPRI measurement, a total internal reflection microscope geometry is used with an 814 nm laser to excite traveling wave surface plasmon polaritons (SPPs) onto a 45 nm gold thin film attached to a microscope slide cover. Upon exposure to an aqueous solution of nanoparticles, SPRI reflectivity images (100 μm x 100 μm) are obtained every 3 s from this microscope for 10 min. These images are subtracted sequentially from each other to create a set of 200 SPRI differential reflectivity ($\Delta\%$ R) images.

Two examples of these 3 s SPRI differential reflectivity images obtained during the exposure of a gold thin film to solutions of HNPs and DNA−HNPs is shown in Figure 2. The

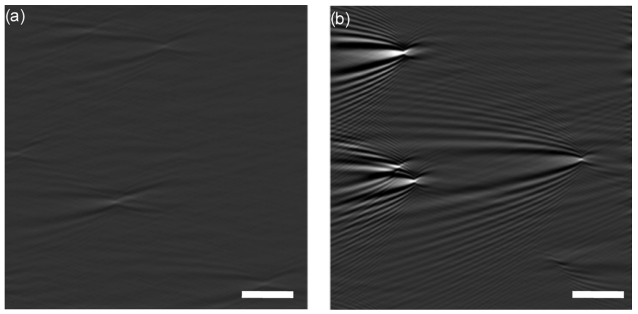

Figure 2. Example of SPRI differential reflectivity images of (a) HNPs and (b) DNA−HNPs, irreversibly adsorbing to the gold thin film surface. The scale bar for both images is 10 μm.

gold has been modified with a 1-undecanethiol monolayer to create a hydrophobic surface onto which both nanoparticles irreversibly adsorb through hydrophobic forces. Each irreversible nanoparticle binding event on the gold surface in the 3 s time window creates a distinctive point diffraction pattern in the image due to the interaction of the nanoparticle refractive index with the traveling SPPs. The shape and intensity of these diffraction patterns have been modeled and quantitated previously;[31,32] the intensity of each DNA−HNP binding event can be quantitated to obtain a single-nanoparticle reflectivity change value, $\Delta\%$ R_{NP}. We have shown in previous papers that $\Delta\%$ R_{NP} depends on both the size and composition of the adsorbed nanoparticle. As such, $\Delta\%$ R_{NP} can be thought of as the "integrated refractive index" of the adsorbed nanoparticle. A collection of 300−400 $\Delta\%$ R_{NP} values for synthesized DNA−HNPs was obtained over several experiments, and results are summarized in Table 2 along with DLS size distribution measurements.

Figure 3 plots two data sets of $\Delta\%$ R_{NP} values obtained from two different group experiments, one for the adsorption of HNPs without DNA incorporation (D0) and one for the adsorption of D1-HNPs, both as a function of time. The two types of HNPs have significantly different average $\Delta\%$ R_{NP} values (which we denote $\langle\Delta\%\ R_{NP}\rangle$) of 0.51 ± 0.02% for D0-HNPs and 5.18 ± 0.22% for D1-HNPs, with ranges represented as 95% confidence intervals. The addition of acrylamide-modified ssDNA to the NIPAm polymerization has led to an almost 10-fold increase in $\langle\Delta\%\ R_{NP}\rangle$. In contrast, DLS measurements on the two types of nanoparticles show

DOI: 10.1021/acs.jpcc.9b00444
J. Phys. Chem. C 2019, 123, 6090−6096

Table 2. Hydrodynamic Size Measurements from DLS for Hydrogel Nanoparticles and Statistics from Single-Nanoparticle SPRI Measurements for Hydrogel Nanoparticles

nanoparticle	diameter (nm)	$\langle \Delta\% R_{NP} \rangle$	standard deviation (s)	95% CI	# of NPs
D0-HNP	246 ± 3	0.51	0.16	0.02	357
D1-HNP	234 ± 5	5.18	2.04	0.22	320
D2-HNP	202 ± 2	2.38	1.17	0.11	424
D3-HNP	216 ± 1	0.59	0.32	0.32	304
D4-HNP	196 ± 3	2.11	0.98	0.10	403
D1-HNP + exonuclease I		3.16	2.09	0.31	180

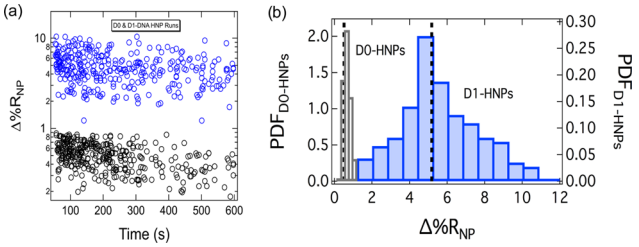

Figure 3. (a) Time-dependent distribution of $\Delta\% R_{NP}$ values of HNPs with (blue) and without (black) DNA incorporation, measured in separate experiments. Each circle represents the $\Delta\% R_{NP}$ for a single HNP, irreversibly adsorbing to the chemically modified surface. (b) $\Delta\% R_{NP}$ frequency distribution histograms obtained from the SPRI adsorption measurements of HNPs (transparent gray bars) and DNA−HNPs (blue bars). The averages for each distribution are denoted by the dotted black lines within each distribution. Average $\Delta\% R_{NP}$ for HNPs and DNA−HNPs are 0.51 ± 0.02 and 5.18 ± 0.22%, respectively.

only a slight change in the nanoparticle diameter from 246 ± 3 to 234 ± 5 nm for D0-HNPs and D1-HNPs, respectively. Cryo-TEM images of D1-HNPs were collected also to show that the particles are not aggregating together and to further corroborate their sizes, as demonstrated in Figure 4.

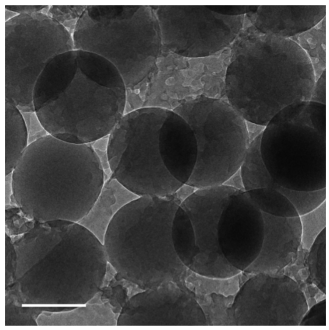

Figure 4. Cryo-TEM image of vitrified D1-HNPs. The scale bar is 200 nm.

The large increase in $\langle \Delta\% R_{NP} \rangle$ when comparing D0-HNPs with D1-HNPs is due to an increase in both nanoparticle density and refractive index in the presence of acrylamide-modified ssDNA (Figure 3). This large increase strongly suggests that (i) a significant amount of 30 mer ssDNA has been incorporated into the D1-HNP and (ii) the presence of the acrylamide-modified ssDNA during polymerization has altered the structure of the hydrogel in a manner that has increased its density. Surprisingly, the increase in $\langle \Delta\% R_{NP} \rangle$, is significantly less for 30 mer sequences that contain more thymine nucleotides: for D2-HNPs, which have over half of the 30 mer nucleotide sequence replaced by thymine, the signal drops to 2.38 ± 0.11%, and for D3-HNPs, which incorporate a 30 mer poly-T ssDNA, the signal drops all of the way down to 0.59 ± 0.03%, just slightly larger than that for the D0-HNPs. These additional measurements strongly suggest that the large increase in $\langle \Delta\% R_{NP} \rangle$ for the DNA−HNPs can be attributed to previously observed Michael addition reactions of the acrylamide with adenine, cytosine, and guanine nucleotides during the polymerization process.[27,29,36] Thymine nucleotides do not react with acrylamide at physiological pH and thus there is no incorporation of the poly-T ssDNA into the D3-HNPs.[27] This is further corroborated by the observed incorporation of 30 mer poly-A ssDNA into the D4 HNPs, where the signal once again increases since adenine is capable of undergoing a Michael addition reaction. The reaction of acrylamide with A, C, and G in the ssDNA greatly assists in the overall incorporation of ssDNA into the nanoparticle and also provides additional cross-linking of the ssDNA and hydrogel. A second potential mechanism for sequence-dependent ssDNA incorporation would be the formation of self-complementary secondary structures between ssDNAs that lead to greater packing and thus denser incorporation of ssDNA into the HNPs. These interactions are typically much weaker, and DNA-folding calculations are shown to have a free energy of −0.98 kcal/mol,[37] proving that the D1 sequence does not show a large degree of folding or secondary structure.

Hybridization Uptake of Complementary ssDNA by DNA−HNPs. To determine the ability of the DNA−HNPs to uptake and hybridize complementary ssDNA from solution, we employed a combination of fluorescence and single-nanoparticle SPRI measurements. Using D1-HNPs, fluorescence loss measurements were performed using fluorescently labeled complementary DNA (D1c) to estimate the loading capacity of DNA into the HNPs. On average, approximately 20 000 fluorophore-modified ssDNAs were incorporated into the DNA−HNPs. Further details are given in the Supporting Information.

To verify that the incorporation of complementary D1c into the D1-HNPs was due to hybridization to form dsDNA, fluorescence measurements using the intercalation of SYBR Green I into dsDNA were performed to demonstrate duplex formation in the DNA−HNPs.

The fluorescence spectrum of DNA−HNPs with either complementary (solid blue line) or noncomplementary (dotted black line) ssDNA, both at a 10 nM solution, is shown in Figure 5. SYBR Green I preferentially stains dsDNA formations, and, as seen in Figure 5, a strong fluorescence signal was only observed in the presence of complementary ssDNA. These results demonstrate that the uptake of complementary ssDNA into the DNA−HNPs is driven by duplex formation to create dsDNA.

Single-nanoparticle SPRI measurements were used to quantitate the hybridization uptake of complementary

DOI: 10.1021/acs.jpcc.9b00444
J. Phys. Chem. C 2019, 123, 6090−6096

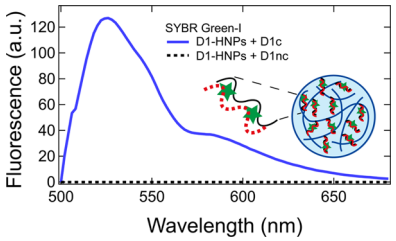

Figure 5. Fluorescence spectra of D1-HNPs in the presence of SYBR Green I dye and either complementary (D1c) or noncomplementary (D1nc) ssDNA. D1-HNPs were mixed initially with either of the ssDNA, followed by the fluorescent dye. Parallel measurements were then performed after three centrifuge/wash cycles before D1-HNP mixtures were resuspended in buffer solution. The solid blue curve indicated the formation of dsDNA within D1-HNPs with its complementary sequence, D1c, and SYBR Green staining. No fluorescence was observed in the D1nc mixture (dotted black line), as SYBR Green preferentially stains dsDNA formations.

ssDNA into the D1-HNPs. Figure 6 shows the change in the $\Delta\%\ R_{NP}$ distribution of the DNA−HNPs after exposure to a

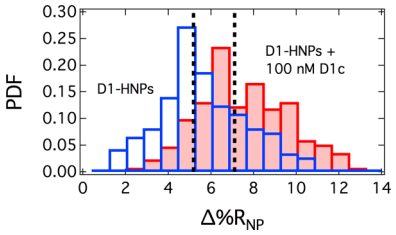

Figure 6. $\Delta\%\ R_{NP}$ frequency distribution histograms obtained from the SPRI adsorption measurements of D1-HNPs onto Au surfaces. The transparent blue bars indicate D1-HNPs before exposure to its complementary sequence, D1c. When exposed to D1c, D1-HNPs uptake the ssDNA, causing a shift in the $\Delta\%\ R_{NP}$ signal, shown as solid red bars. The dotted black lines for each distribution denote the averages, 5.18 ± 0.22 and 7.11 ± 0.25% for D1-HNPs and D1-HNPs in the presence of D1c, respectively.

100 nM complementary ssDNA solution. The average $\langle\Delta\%\ R_{NP}\rangle$ increased by approximately 2% (from 5.18 ± 0.22 to 7.11 ± 0.25%). As a control experiment, negligible change in $\langle\Delta\%\ R_{NP}\rangle$ was observed for DNA−HNPs in the presence of 100 nM noncomplementary ssDNA. These SPRI measurements confirm the ability of these HNPs to incorporate ssDNA; however, only a 2% increase in $\langle\Delta\%\ R_{NP}\rangle$ suggests that just 35% of the DNA is accessible for sequence-specific hybridization.

Additional single nanoparticle SPRI measurements were performed to determine the concentration dependence of the hybridization uptake of complementary ssDNA into the DNA−HNPs. The change in the average $\langle\Delta\%\ R_{NP}\rangle$ for the DNA−HNPs is plotted against the log of complementary ssDNA concentration in Figure 7. The solid red line in the figure is a fit of this concentration dependence to a Langmuir adsorption isotherm. The Langmuir adsorption coefficient for this fit is $4.89 \times 10^8\ M^{-1}$; the inverse of this number, about 2 nM, is the concentration for which half of the adsorption sites are filled. The value for the Langmuir adsorption coefficient is approximately 5−10 times higher than that observed for the adsorption of complementary ssDNA to ssDNA monolayers on gold thin films;[31] this result suggests that duplex formation is more favorable in the DNA−HNPs as compared to that on a

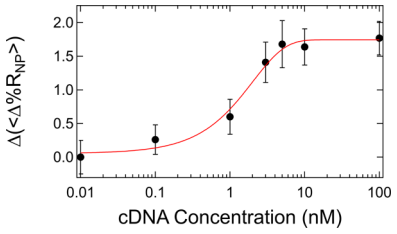

Figure 7. Langmuir isotherm fit of the change in $\langle\Delta\%\ R_{NP}\rangle$, comparing unoccupied D1-HNPs with D1-HNPs loaded with D1c. Each measurement is the difference between the $\Delta\%\ R_{NP}$ signal concentration at a D1c concentration and empty D1-HNPs. The adsorption constant K_{ads} was determined to be $4.89 \times 10^8\ M^{-1}$.

surface, most likely due to the increased flexibility and access of the ssDNA in the three-dimensional hydrogel format.

Enzymatic Hydrolysis of ssDNA in DNA−HNPs. As a demonstration of the bioavailability of the ssDNA in the HNPs, SPRI measurements were used to monitor the enzymatic hydrolysis of the ssDNA in the nanoparticles. The DNA enzyme exonuclease I will exclusively hydrolyze ssDNA but not dsDNA. SPRI nanoparticle measurements were performed on DNA−HNPs after exposure to a solution of exo I for 1 h; Figure 8 plots $\Delta\%\ R_{NP}$ distributions for pre-

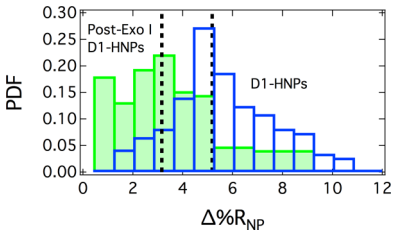

Figure 8. Single-nanoparticle SPRI frequency distributions comparing DNA−HNP distributions before (transparent blue bars) and after (solid green bars) exposure to exonuclease I. The dotted lines for each distribution represent the $\Delta\%\ R_{NP}$ averages for pre-exposure and postexposure, 5.18 ± 0.22 and 3.16 ± 0.31%, respectively.

exposure (blue bars) and postexposure (green bars) of exo I. A significant decrease in $\langle\Delta\%\ R_{NP}\rangle$ was observed, dropping the value from 5.18 to 3.16 ± 0.31% after enzymatic activity; we attribute this decrease to the hydrolysis of ssDNA in the DNA−HNP. Interestingly, this decrease in $\langle\Delta\%\ R_{NP}\rangle$ is approximately of the same value as the maximum amount of increase in $\langle\Delta\%\ R_{NP}\rangle$ observed in hybridization adsorption experiments in Figure 7, maintaining roughly the same percentage of accessibility as DNA duplex formation.

CONCLUSIONS AND FUTURE DIRECTIONS

In conclusion, we have shown in this paper that DNA−HNPs can be prepared via the incorporation of acrylamide-modified 30 mer ssDNA and that they can be used to uptake complementary ssDNA by hybridization adsorption/incorporation. Moreover, the ssDNA in the DNA−HNPs can undergo enzymatic hydrolysis, demonstrating the availability of the incorporated ssDNA to enzymatic activity. An almost 10-fold increase is observed in average $\langle\Delta\%\ R_{NP}\rangle$ for the D1-HNPs as compared to that for the HNPs without ssDNA; this large increase is attributed to both the inclusion of acrylamide-modified ssDNA into the hydrogel and its effect on the polymerization process. Specifically, the Michael addition of

DOI: 10.1021/acs.jpcc.9b00444
J. Phys. Chem. C 2019, 123, 6090−6096

acrylamide to A, C, and G nucleotides in the ssDNA assisted in the incorporation of DNA into the DNA−HNPs. However, this reaction limited the bioavailability of the ssDNA within DNA−HNPs to about 35%. Future work will focus on the further synthesis, nucleic acid/protein uptake, and enzymatic activity of various ssDNA sequences, such as aptamers, in these DNA−HNPs.

■ ASSOCIATED CONTENT

Supporting Information

The Supporting Information is available free of charge on the ACS Publications website at DOI: 10.1021/acs.jpcc.9b00444.

SYBR Green I fluorescence measurements and fluorescence loss measurements, fluorescence curve was plotted to calculate the fluorescence of the supernatant (Figure S1), statistical data for SPRI adsorption measurements, SPRI microscopy for D1c binding to D1-HNPs (Table S1) (PDF)

■ AUTHOR INFORMATION

Corresponding Author

*E-mail: rcorn@uci.edu.

ORCID

Adam M. Maley: 0000-0003-1851-984X

Robert M. Corn: 0000-0002-4756-2161

Present Address

[†]Department of Pathology, Brigham and Women's Hospital, Harvard Medical School, Boston, MA 02115, USA Wyss Institute for Biologically Inspired Engineering, Harvard University, Boston, MA 02115.

Notes

The authors declare no competing financial interest.

■ ACKNOWLEDGMENTS

This work was supported by the National Science Foundation through grant CHE-1807317. DLS and nanoparticle size distribution and concentration data were acquired at the Laser Spectroscopy Facility in the Department of Chemistry at UC, Irvine. The authors would like to thank Christian Baca for his assistance in data acquisition and analysis and Dr Li Xing for her help in acquiring cryo-TEM images. Cryo-TEM work was performed at the UC Irvine Materials Research Institute (IMRI).

■ REFERENCES

(1) Zhang, Z.; Liu, J. Intracellular delivery of a molecularly imprinted peroxidase mimicking DNAzyme for selective oxidation. *Mater. Horiz.* **2018**, *5*, 738−744.

(2) Huang, Y.; Ma, Y.; Chen, Y.; Wu, X.; Fang, L.; Zhu, Z.; Yang, C. J. Target-responsive DNAzyme cross-linked hydrogel for visual quantitative detection of lead. *Anal. Chem.* **2014**, *86*, 11434−11439.

(3) Karimi, M.; Ghasemi, A.; Sahandi Zangabad, P.; Rahighi, R.; Moosavi Basri, S. M.; Mirshekari, H.; Amiri, M.; Shafaei Pishabad, Z.; Aslani, A.; Bozorgomid, M.; et al. Smart micro/nanoparticles in stimulus-responsive drug/gene delivery systems. *Chem. Soc. Rev.* **2016**, *45*, 1457−1501.

(4) Kahn, J. S.; Hu, Y.; Willner, I. Stimuli-responsive DNA-based hydrogels: From basic principles to applications. *Acc. Chem. Res.* **2017**, *50*, 680−690.

(5) Peppas, N. A.; Hilt, J. Z.; Khademhosseini, A.; Langer, R. Hydrogels in biology and medicine: From molecular principles to bionanotechnology. *Adv. Mater.* **2006**, *18*, 1345−1360.

(6) Carvalho, W. S. P.; Wei, M.; Ikpo, N.; Gao, Y.; Serpe, M. J. Polymer-based technologies for sensing applications. *Anal. Chem.* **2018**, *90*, 459−479.

(7) Hamidi, M.; Azadi, A.; Rafiei, P. Hydrogel nanoparticles in drug delivery. *Adv. Drug Delivery Rev.* **2008**, *60*, 1638−1649.

(8) Vermonden, T.; Censi, R.; Hennink, W. E. Hydrogels for protein delivery. *Chem. Rev.* **2012**, *112*, 2853−2888.

(9) Segovia, N.; Pont, M.; Oliva, N.; Ramos, V.; Borros, S.; Artzi, N. Hydrogel doped with nanoparticles for local sustained release of siRNA in breast cancer. *Adv. Healthcare Mater.* **2015**, *4*, 271−280.

(10) Plamper, F. A.; Richtering, W. Functional microgels and microgel systems. *Acc. Chem. Res.* **2017**, *50*, 131−140.

(11) Cho, K.; Fasoli, J. B.; Yoshimatsu, K.; Shea, K. J.; Corn, R. M. Measuring melittin uptake into hydrogel nanoparticles with near-infrared single nanoparticle surface plasmon resonance microscopy. *Anal. Chem.* **2015**, *87*, 4973−4979.

(12) O'Brien, J.; Lee, S.-H.; Gutiérrez, J. M.; Shea, K. J. Engineered nanoparticles bind elapid snake venom toxins and inhibit venom-induced dermonecrosis. *PLoS Neglected Trop. Dis.* **2018**, *12*, No. e0006736.

(13) Miura, Y.; Hoshino, Y.; Seto, H. Glycopolymer nanobiotechnology. *Chem. Rev.* **2016**, *116*, 1673−1692.

(14) Maley, A. M.; Terada, Y.; Onogi, S.; Shea, K. J.; Miura, Y.; Corn, R. M. Measuring protein binding to individual hydrogel nanoparticles with single-nanoparticle surface plasmon resonance imaging microscopy. *J. Phys. Chem. C* **2016**, *120*, 16843−16849.

(15) Chen, Y.; Nakamoto, K.; Niwa, O.; Corn, R. M. On-chip synthesis of RNA aptamer microarrays for multiplexed protein biosensing with SPR imaging measurements. *Langmuir* **2012**, *28*, 8281−8285.

(16) Freeman, R.; Liu, X. Q.; Willner, I. Amplified multiplexed analysis of DNA by the Exonuclease III-catalyzed regeneration of the target DNA in the presence of functionalized semiconductor quantum dots. *Nano. Lett.* **2011**, *11*, 4456−4461.

(17) Frutos, A. G.; Smith, L. M.; Corn, R. M. Enzymatic ligation reactions of DNA "words" on surfaces for DNA computing. *J. Am. Chem. Soc.* **1998**, *120*, 10277−10282.

(18) Lilienthal, S.; Shpilt, Z.; Wang, F.; Orbach, R.; Willner, I. Programmed DNAzyme-triggered dissolution of DNA-based hydrogels: Means for controlled release of biocatalysts and for the activation of enzyme cascades. *ACS Appl. Mater. Interfaces* **2015**, *7*, 8923−8931.

(19) Song, S.; Wang, L.; Li, J.; Fan, C.; Zhao, J. Aptamer-based biosensors. *TrAC, Trends Anal. Chem.* **2008**, *27*, 108−117.

(20) Breaker, R. R.; Joyce, G. F. A DNA enzyme with Mg2+-dependent RNA phosphoesterase activity. *Chem. Biol.* **1995**, *2*, 655−660.

(21) Moura, L. M.; Martinho, J. M. G.; Farinha, J. P. S. DNA hybridization in thermoresponsive polymer nanoparticles. *ChemPhysChem* **2010**, *11*, 1749−1756.

(22) Fujita, M.; Hiramine, H.; Pan, P.; Hikima, T.; Maeda, M. Effects of complementary DNA and Salt on the thermoresponsiveness of Poly(N-isopropylacrylamide)-b-DNA. *Langmuir* **2016**, *32*, 1148−1154.

(23) Soontornworajit, B.; Zhou, J.; Shaw, M. T.; Fan, T. H.; Wang, Y. Hydrogel functionalization with DNA aptamers for sustained PDGF-BB release. *Chem. Commun.* **2010**, *46*, 1857−1859.

(24) Smith, M. H.; Lyon, L. A. Multifunctional nanogels for siRNA delivery. *Acc. Chem. Res.* **2012**, *45*, 985−993.

(25) Dunn, S. S.; Tian, S.; Blake, S.; Wang, J.; Galloway, A. L.; Murphy, A.; Pohlhaus, P. D.; Rolland, J. P.; Napier, M. E.; DeSimone, J. M. Reductively responsive siRNA-conjugated hydrogel nanoparticles for gene silencing. *J. Am. Chem. Soc.* **2012**, *134*, 7423−7430.

(26) Zeynep Atay, N.; Çalgan, D.; Özakat, E.; Varnali, T. Acrylamide and glycidamide adducts of Guanine. *J. Mol. Struct.: THEOCHEM* **2005**, *728*, 249−251.

(27) Besaratinia, A.; Pfeifer, G. P. DNA adduction and mutagenic properties of acrylamide. *Mutat. Res., Genet. Toxicol. Environ. Mutagen.* **2005**, *580*, 31−40.

DOI: 10.1021/acs.jpcc.9b00444
J. Phys. Chem. C 2019, 123, 6090−6096

(28) Watzek, N.; Böhm, N.; Feld, J.; Scherbl, D.; Berger, F.; Merz, K. H.; Lampen, A.; Reemtsma, T.; Tannenbaum, S. R.; Skipper, P. L.; et al. N7-glycidamide-guanine DNA adduct formation by orally ingested acrylamide in rats: A dose−response study encompassing human diet-related exposure levels. *Chem. Res. Toxicol.* **2012**, *25*, 381−390.
(29) Huang, S.; Lu, S.; Huang, C.; Sheng, J.; Zhang, L.; Su, W.; Xiao, Q. An electrochemical biosensor based on single-stranded DNA modified gold electrode for acrylamide determination. *Sens. Actuators, B* **2016**, *224*, 22−30.
(30) Freeman, R.; Han, M.; Álvarez, Z.; Lewis, J. A.; Wester, J. R.; Stephanopoulos, N.; McClendon, M. T.; Lynsky, C.; Godbe, J. M.; Sangji, H.; et al. Reversible self-assembly of superstructured networks. *Science* **2018**, *362*, 808−813.
(31) Halpern, A. R.; Wood, J. B.; Wang, Y.; Corn, R. M. Single-nanoparticle near-infrared surface plasmon resonance microscopy for real-time measurements of DNA hybridization adsorption. *ACS Nano* **2014**, *8*, 1022−1030.
(32) Maley, A. M.; Lu, G. J.; Shapiro, M. G.; Corn, R. M. Characterizing single polymeric and protein nanoparticles with surface plasmon resonance imaging measurements. *ACS Nano* **2017**, *11*, 7447−7456.
(33) Zybin, A.; Kuritsyn, Y. A.; Gurevich, E. L.; Temchura, V. V.; Uberla, K.; Niemax, K. Real-time detection of single immobilized nanoparticles by surface plasmon resonance imaging. *Plasmonics* **2010**, *5*, 31−35.
(34) Wang, W.; Tao, N. Detection, counting, and imaging of single nanoparticles. *Anal. Chem.* **2014**, *86*, 2−14.
(35) Yu, H.; Shan, X.; Wang, S.; Tao, N. Achieving high spatial resolution surface plasmon resonance microscopy with image reconstruction. *Anal. Chem.* **2017**, *89*, 2704−2707.
(36) Solomon, J. J.; Fedyk, J.; Mukai, F.; Segal, A. Direct alkylation of 2′-Deoxynucleosides and DNA following in vitro reaction with acrylamide. *Cancer Res.* **1985**, *45*, 3465−3470.
(37) Gruber, A. R.; Lorenz, R.; Bernhart, S. H.; Neuböck, R.; Hofacker, I. L. The Vienna RNA websuite. *Nucleic Acids Res.* **2008**, *36*, W70−W74.

DOI: 10.1021/acs.jpcc.9b00444
J. Phys. Chem. C 2019, 123, 6090−6096